Journal of Materials Chemistry C

ROYAL SOCIETY OF CHEMISTRY

PAPER

View Article Online
View Journal | View Issue

Open Access Article. Published on 24 May 2022. Downloaded on 5/20/2026 3:52:14 PM.
This article is licensed under a Creative Commons Attribution 3.0 Unported Licence.

Check for updates

Cite this: J. Mater. Chem. C, 2022, 10, 8955

Critical analysis of self-doping and water-soluble n-type organic semiconductors: structures and mechanisms†

Lewis M. Cowen,*[a] Peter A. Gilhooly-Finn,[ab] Alexander Giovannitti,[c] Garrett LeCroy,[c] Harry Demetriou,[d] William Neal,[b] Yifan Dong,[a] Megan Westwood,[a] Sally Luong,[e] Oliver Fenwick,[e] Alberto Salleo,[c] Sandrine Heutz,[d] Christian B. Nielsen[b] and Bob C. Schroeder*[a]

Received 18th March 2022,
Accepted 17th May 2022

DOI: 10.1039/d2tc01108e

rsc.li/materials-c

Self-doping organic semiconductors provide a promising route to avoid instabilities and morphological issues associated with molecular n-type dopants. Structural characterization of a naphthalenetetracarboxylic diimide (NDI) semiconductor covalently bound to an ammonium hydroxide group is presented. The dopant precursor was found to be the product of an unexpected base catalyzed hydrolysis, which was reversible. The reversible hydrolysis had profound consequences on the chemical composition, morphology, and electronic performance of the doped films. In addition, we investigated the degradation mechanism of the quaternary ammonium group and the subsequent doping of NDI. These findings reveal that the products of more than one chemical reaction during processing of films must be considered when utilizing this promising class of water-soluble semiconductors.

Introduction

The introduction of charges on to organic semiconductors through doping with an external molecular species is vital for their use in various applications. The requirement for low ionization potentials (IP) in n-type dopants means that their application has been slow when compared to their p-type counter-parts.[1] Organic photovoltaics (OPV),[2] thermoelectrics (OTE)[3,4] and field effect transistors (OFET)[5] are all reliant upon, or their performance can be improved by, efficient doping of the n-type component. A more thorough understanding of the chemical structures, transformations and charge transfer processes undergone between n-type semiconductors and dopants is therefore important for future commercial success of these various fields.

One major obstacle to efficient n-type doping systems has been the instability of dopants and doped semiconductors. Dopants with small solid-state ionization potentials (IP), typically less than 4.0 eV, are capable of reducing O_2 to O^{2-} and H_2O to HO^- under atmospheric conditions. Similarly, doped n-type semiconductors require very large electron affinities (EA) to prevent oxidation of the excited state.[6,7] Problems are therefore encountered in their handling and experimental studies are mostly limited to glove-box work. To avoid this, successful n-type dopants are normally generated from a stable precursor. For example, stable 18 electron dimers of metallocenes are often cleaved to give the 19 electron metallocene as dopant.[8,9] Similarly, 2,3-dihydro-1*H*-benzoimidazoles (DMBI-H)[10–13] and triaminomethanes (TAM)[14] are not active dopants but donate hydrides which reduce organic semiconductors.

Quaternary ammonium halide dopant precursors, covalently bound to a perylenetetracarboxylic diimide (PDI) aromatic acceptor, have been designed in an effort to produce n-type organic semiconductors which experience minimal morphological disruption upon doping. Reducing the stable ammonium halide precursor with sodium metal leads to the zwitterionic doped semiconductor. Blends of the zwitterionic doped species and a neutral PDI derivative exhibited conductivities of 10 mS cm^{-1}.[15,16] The introduction of covalently bound quaternary ammonium groups is an attractive prospect

[a] Department of Chemistry, University College London, London, WC1H 0AJ, UK. E-mail: lewis.cowen.17@ucl.ac.uk, b.c.schroeder@ucl.ac.uk
[b] Department of Chemistry, Queen Mary University of London, Mile End Road, London, E1 4NS, UK
[c] Department of Materials Science and Engineering, Stanford University, Stanford, CA 94305, USA
[d] Department of Materials and London Centre for Nanotechnology, Imperial College London, London SW7 2AZ, UK
[e] School of Engineering and Materials Science, Queen Mary University of London, London, E1 4NS, UK

† Electronic supplementary information (ESI) available: Chemicals and instrument details, detailed synthetic procedures, structural characterisation, NMR spectra, cyclic voltammetry, EPR spectra, GIWAXS data, electrical characterization and an overview of the NDI-TEG and tertiary amine doping study. See DOI: https://doi.org/10.1039/d2tc01108e

Open Access Article. Published on 24 May 2022. Downloaded on 5/20/2026 3:52:14 PM.
This article is licensed under a Creative Commons Attribution 3.0 Unported Licence.

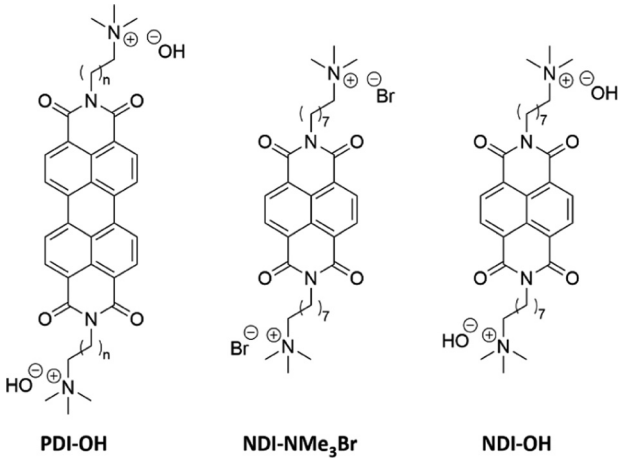

Fig. 1 Structure of previously studied PDI–OH[21–23] as well as the halide precursor **NDI-NMe$_3$Br** and **NDI-OH** reported here.

due to their charged nature, allowing for processing from more environmentally friendly solvents such as water without the use of additives.[17] Furthermore the use of orthogonal solvent systems facilitates device fabrication, as miscibility between dopant and semiconductor in the solid state is avoided.[18–20] Quaternary ammonium hydroxide moieties have been bound to rylene diimides and, upon dehydration of aqueous films, absorption spectra indicating the presence of charge carriers were recorded.[21] An ion-exchange column was used to exchange a halide precursor for the hydroxyl counterion, shown as PDI-OH in Fig. 1. The resultant aqueous solution was found to be stable under ambient conditions and formed conductive homogeneous films upon dehydration. It was suggested that the driving force behind doping was the loss of solvation energy around the hydroxyl anion upon film formation, subsequently the negative charge was transferred to the more polarizable PDI core. By altering the alkyl spacer length, *n*, between the PDI core and the quaternary ammonium moiety, PDI–OH has exhibited maximum electrical conductivities, σ, of 0.5 S cm^{-1}.[22] A mechanism of doping has been investigated involving the demethylation of the ammonium, leaving a dimethylamine group bound to the PDI sidechain.[23] The resultant dimethylamine was suggested to be the doping moiety. This was evidenced by a growth in X-ray photoelectron spectroscopy (XPS) signal for NMe_2 nitrogen upon film annealing while the NMe_3^+ signal diminished. Photo-[24–26] and thermal-induced[27] electron transfers between bound tertiary amines and rylene diimide semiconductors have previously been observed.

It is possible however that the quaternary ammonium end group degrades *via* alternative routes. Previously degradation has been shown to favor an E2 Hofmann elimination when β-hydrogens are present and sterically available for abstraction.[28–31] This would result in a tertiary amine, trimethylamine (TMA), as well as a terminal alkene on the semiconductor side chain.

In order to further elucidate the chemical pathways through which quaternary amines act as n-type dopants to bound rylene diimides, we synthesized the compound *N*,*N*′-bis(8-(trimethylammoniumbromide)octylene)-1,4,5,8-naphthalenetetracarboxylic diimide (**NDI-NMe$_3$Br**, Fig. 1). As the aim of this study is to gain deeper insights into the underlying doping chemistry of quaternary amine functionalized rylene diimides, rather than to maximize electrical conductivity, NDI was chosen as the semiconducting building block rather than PDI. In case of unexpected chemical reactions during the doping mechanism, the NDI core will favor the formation of a lesser number of isomers, thereby facilitating the structural characterization compared to PDI derivatives. The halide counterion was exchanged for a hydroxide *via* ion-exchange resin to give an aqueous solution of the dopant precursor, *N*,*N*′-bis(8-(trimethylammoniumhydroxide)octylene)-1,4,5,8-naphthalene-tetracarboxylic diimide (**NDI-OH**, Fig. 1). Using an NDI aromatic core, rather than PDI, allows for increased solubility and simplified analysis of solution spectroscopic measurements at the expense of a decreased conjugation length in the semiconducting core. This trade-off between potentially decreased electronic performance, in NDI compared to PDI, and ease of analysis was considered worthwhile, since the aim of this study was primarily focused on structural characterization of **NDI-OH** and determination of the role of the quaternary ammonium group in doping, rather than optimizing electrical conductivity.

A combination of nuclear magnetic resonance (NMR) and infra-red (IR) spectroscopies, as well as mass-spectrometry, have been used to confirm the structure of the dopant precursor for the first time as well as analyse the product of doping upon drying. These structural characterizations revealed that dynamic reactions involving the NDI imide group play a part in the composition of doped films. An insight into how the complex reactions involving NDI and quaternary ammonium groups affects film morphology was investigated through atomic force microscopy (AFM) and grazing incidence wide angle X-ray scattering (GIWAXS) measurements. In combination with this ultraviolet-visible (UV-vis) absorption spectroscopy, electron paramagnetic resonance (EPR) spectroscopy and four-point probe conductivity measurements, have been used to help probe both the mechanism and efficiency of intramolecular charge transfer.

Results and discussion

Synthesis and characterisation of NDI-OH

Two synthetic routes to the quaternary ammonium halides **5** and **NDI-NMe$_3$Br** are outlined in Scheme 1. Napthalenetetracarboxylic dianhydride (**1**) was reacted with ammonium acetate to give naphthalenetetracarboxylic diimide (**2**). A Mitsunobu type reaction was then used to give the *N*-bromooctyl functionalized product **3**. The initial target was the quaternary ammonium iodide product **5**, however the dimethylamine intermediate **4** was found to be unstable, likely through an intramolecular photoinduced electron transfer.[24] **5** was therefore synthesized *via* a one-pot reaction in which the S_N2 substitution to give **4** was followed immediately by quaternization with methyl iodide. This made the separation of pure **5** from the reaction mixture difficult and the quaternary ammonium halide target was changed to **NDI-NMe$_3$Br**. Quaternization *via* this route was achieved by

Open Access Article. Published on 24 May 2022. Downloaded on 5/20/2026 3:52:14 PM.
This article is licensed under a Creative Commons Attribution 3.0 Unported Licence.

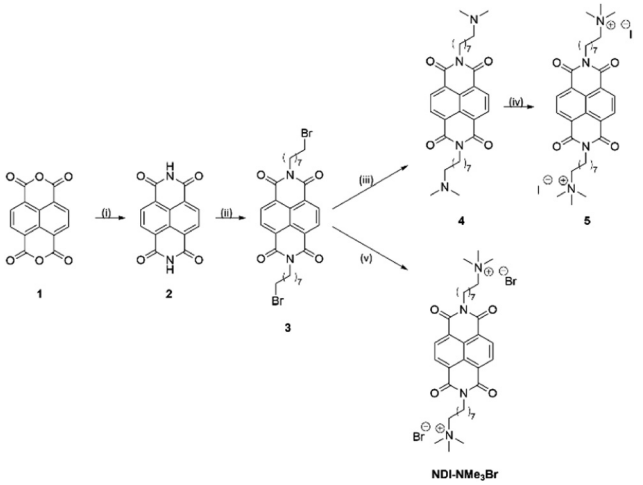

Scheme 1 Synthesis of quaternary ammonium halides 5 and **NDI-NMe$_3$Br**. Reagents and conditions: (i) NH_4OAc, AcOH, reflux 1 h, 72% (ii) 8-bromooctan-1-ol, DEAD, PPh_3, THF, 14 h, 21% (iii) $NHMe_2$, THF, reflux 16 h, (iv) MeI, $CHCl_3$, reflux 2 h, 44% combined yield with (iii). (v) NMe_3·HCl, $NaHCO_3$, MeCN, 80 °C, 12 h, 51%.

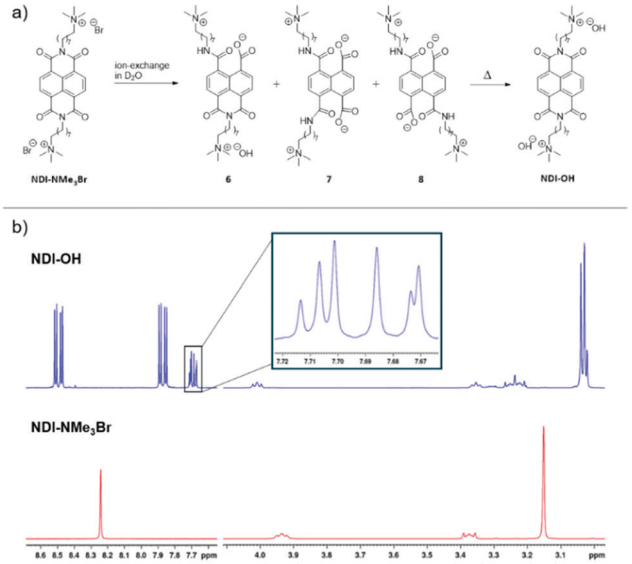

Fig. 2 (a) Hydrolysis of **NDI-NMe$_3$Br** to give a mixture of products. (b) Solution ^{1}H NMR spectra of **NDI-NMe$_3$Br** (bottom) and hydrolysed **NDI-OH** mixture (top) in deuterium oxide. Inset shows signals attributed to the doubly hydrolysed *syn* (7) and *anti* (8) products.

reaction of **3** with the salt trimethylamine hydrochloride under basic conditions to yield **NDI-NMe$_3$Br**. The presence of predominantly bromide counterion, rather than chloride, was confirmed by X-ray fluorescence (XRF) spectroscopy and results are summarised in Table S1 of the ESI.† Bromine was detected at a concentration of 94.364% and chlorine at 3.422%. Elements lighter than sodium are difficult to detect by XRF so are not included in the results.

Previously quaternary ammonium hydroxides, such as **NDI-OH**, have been generated by eluting an aqueous solution of a corresponding ammonium halide through a column of hydroxy-form ion exchange resin.[21–23] The resultant aqueous solution has not previously been subjected to any structural analysis, however. To elucidate the chemical structure of **NDI-OH** we first prepared a sample by passing **NDI-NMe$_3$Br** through a column of hydroxy-form ion exchange resin using deuterium oxide as eluent. It was then possible to perform NMR experiments on the resultant solution. Two key identifying regions of the solution ^{1}H NMR spectrum of **NDI-OH** are shown in Fig. 2 and are compared to the same regions for **NDI-NMe$_3$Br**. A singlet corresponding to the four equivalent aromatic protons, normally observed in symmetrical NDI compounds, was seen in **NDI-NMe$_3$Br** at 8.24 ppm. This singlet however was not seen in **NDI-OH** but instead four doublets were observed at 8.51, 8.48, 7.89 and 7.86 ppm. The appearance of these doublets suggests a loss of equivalence in the NDI aromatic hydrogens and the loss of a plane of symmetry in the molecule. The loss of symmetry is also supported by the observation of additional signals at 3.35 ppm and 3.25 ppm in the spectrum for **NDI-OH**. Two further singlets are also observed in the region between 3.04 and 3.02 ppm indicating the presence of additional *N*-methyl hydrogen environments.

When exposed to solutions of aqueous base, the imide group of NDI derivatives are susceptible to ring-opening hydrolysis.[32] This observation provides a rationale for the differences in NMR spectra between **NDI-NMe$_3$Br** and **NDI-OH**. The measured pH of an aqueous solution of **NDI-OH** after eluting through the ion-exchange column was 9.5. When exposed to the basic ion-exchange resin **NDI-NMe$_3$Br** underwent hydrolysis at one or both of its imide groups, the process is summarized in Fig. 2. The majority product, which gives rise to the doublets between 8.52 and 7.85 ppm, is the mono-amide (**6**). Two isolated singlets are observed for the *syn*-product (**7**) at 7.71 and 7.67 ppm, whereas the *anti*-product (**8**) displays two pairs of equivalent hydrogens which give rise to an AB-quartet centered on 7.69 ppm (J = 7.4 Hz).

Full NMR characterization of **NDI-OH**, including ^{1}H, ^{13}C and homonuclear 2D NMR (Fig. S2 to S8, ESI†), further support the claim that **NDI-OH** in solution is a mixture of products of base catalyzed hydrolysis. In addition to this electron-spray ionization mass spectrometry (ESI-MS), shown in Fig. S1 (ESI†), gives rise to peaks at 636 m/z and 312 m/z, corresponding to the singly and doubly charged product **6**.

Finally, hydrolysis was also observed in absorption spectra. Fig. 3a shows a comparison between the solution absorption spectra of **NDI-NMe$_3$Br** and **NDI-OH** and the results are summarized in Table 1. The spectrum of **NDI-NMe$_3$Br** closely matches previous NDI derivatives with two absorption maxima at 363 and 383 nm.[32,36] For **NDI-OH** a single absorption band with a small shoulder was observed with maxima at 352 nm. Similar absorption spectra have been observed for 1,8-naphthalamides[37] and have previously been assigned as mono-hydrolysed products when naphthalenediimides were treated with aqueous base.[32] The loss of an imide ring in **NDI-OH**, when compared to **NDI-NMe$_3$Br**, may also lead to a decrease in the electron affinity (EA).[36] This is supported by the results of solution cyclic voltammetry (CV) measurements, shown in Fig. S17 (ESI†) and results are summarized in Table 1. **NDI-NMe$_3$Br** shows

Open Access Article. Published on 24 May 2022. Downloaded on 5/20/2026 3:52:14 PM.
This article is licensed under a Creative Commons Attribution 3.0 Unported Licence.

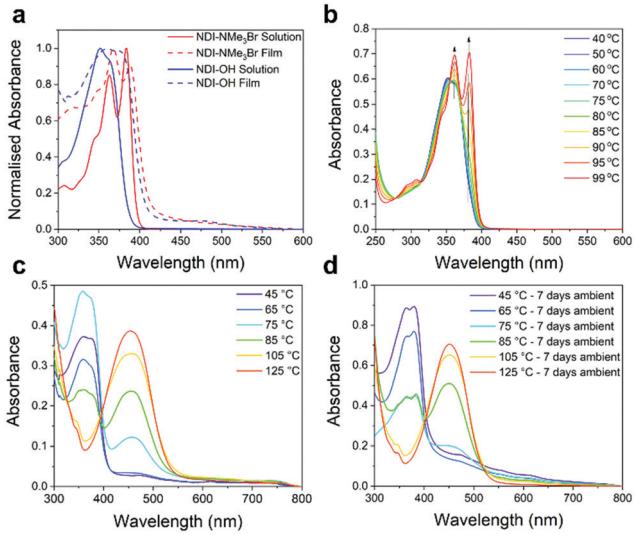

Fig. 3 (a) UV-vis. absorption spectra of aqueous solutions of **NDI-NMe$_3$Br** (solid red) and **NDI-OH** (solid blue) and thin films of **NDI-NMe$_3$Br** (dashed red) and **NDI-OH** (dashed blue). Thin films were made by drop-casting from aqueous solutions at 45 °C. (b) UV-vis. absorption spectra of a solution of **NDI-OH** heated between temperatures of 40 °C and 99 °C. (c) UV-vis. absorption spectra of **NDI-OH** thin-films made by drop-casting a 5 mg mL^{-1} solution at temperatures between 45 °C and 125 °C. (d) UV-vis. absorption spectra of **NDI-OH** thin-films made by drop-casting a 5 mg mL^{-1} solution at temperatures between 45 °C and 125 °C then left under ambient conditions for 7 days.

Table 1 Electrochemical and optical properties of **NDI-NMe$_3$Br** and **NDI-OH**

Compound	$E_{1/2}$[a] (V)	E_{onset}[a] (V)	λ_{max}[b] (nm)	E_g[c] (eV)	EA (eV)	IP[f] (eV)
NDI-NMe$_3$Br	−0.56	n/a	383 386	3.12	4.16[d]	7.28
NDI-OH	n/a	−0.91	352	3.22	3.80[e]	7.02

[a] From solution cyclic voltammetry in water using glassy carbon working electrode, platinum wire counter electrode and Ag/Ag$^+$ reference electrode. Values are reported from the 4th cycle and measured at 100 mV s^{-1}. [b] From solution UV-vis absorption spectroscopy in water. [c] Optical bandgap estimated from absorption band onset of solution UV-vis spectra in Fig. 3a. [d] Estimated using the equation EA = 4.71 + $E_{1/2}$. [e] Estimated using the equation EA = 4.71 + E_{onset}.[33–35] [f] Estimated using equation IP = EA + Optical band gap.

a fully reversible reduction with a half potential ($E_{1/2}$) of −0.56 V. From $E_{1/2}$, and using Ag/Ag$^+$ as reference half-cell, an EA of 4.16 eV was estimated for **NDI-NMe$_3$Br**. The reduction of **NDI-OH** observes quasi-reversibility and therefore the EA was estimated from the onset of reduction (E_{onset}) at −0.91 V. An estimated EA of 3.80 eV was derived for **NDI-OH**, a decrease of 0.36 eV when compared to **NDI-NMe$_3$Br**. This destabilization of the LUMO, as a result of ring-opening hydrolysis, may have a detrimental effect on the **NDI-OH** aromatic core's ability to act as an electron acceptor.

Doped structures of NDI-OH

Previous studies of tethered quaternary ammonium salts have triggered doping either by spin-coating[21] or drop-casting[22,23] the aqueous solution followed by annealing at temperatures of 120 °C or above. The resultant thin films then exhibited maximum electrical conductivities of up to 0.5 S cm^{-1} and red-shifted absorption features indicative of polaron type energy levels within the band gap. To confirm the presence of similar radical type charged species in **NDI-OH**, the aqueous solution was drop-cast and annealed for 40 minutes on pre-heated glass substrates at a range of temperatures between 45 °C and 125 °C. The absorption spectra of thin films are shown in Fig. 3c. At lower drop-casting temperatures (<65 °C), the absorption spectra closely resemble those of **NDI-OH** in solution with one major absorption band at 350 nm. This indicates that films formed at lower drop-casting temperatures are primarily composed of the ring-opened compounds **6**, **7** and **8**.

After drop-casting at higher temperatures (>75 °C) a second absorption feature, with maxima at 458 nm, was observed. As the drop-casting temperature was increased this longer wavelength band intensified while the band at 350 nm continuously decreased in intensity. At 125 °C the shorter wavelength band was completely quenched. The absorption at 458 nm closely matches the previously reported absorbance of NDI radical anions generated both chemically and electrochemically which suggests charge transfer on to the NDI core has occurred.[38,39] However, we cannot in good confidence assign the absorption band at 458 nm solely to the generation of radical anions, as this should have a much more profound impact on the materials charge transport properties discussed below. In our opinion it is more likely that a significant part of this absorption band originates from further, and currently unidentified, chemical changes in the thin films, whose absorption is overshadowing the underlying polaron absorption band, known to arise at similar wavelengths.

Absorption spectra of **NDI-OH** drop-cast films which were left under ambient conditions for seven days (Fig. 3d) show that at higher drop-casting temperatures the longer wavelength absorbance persisted, providing further evidence that NDI radical anions are unlikely the only cause of this absorption band since doped n-types are often air sensitive. It is widely believed that for n-doped semiconductors to avoid oxidation by oxygen in air they require a LUMO level of less than −4.0 eV.[7,38,39] In addition NDI radical anions have been shown to be notoriously difficult to stabilize with only a few successful examples reported in which the NDI aromatic core was functionalized with highly electron withdrawing groups.[27,40–42] Although the electrochemically determined EA of **NDI-OH** was 3.80 eV, this was measured in an aqueous solution and it should not be assumed that doped thin films will have the same EA in the solid state.

In order to investigate the origin of the additional absorption band further, UV-vis absorption spectra were also obtained for an aqueous solution of **NDI-OH** which was heated to 99 °C (b). At no point was an absorption at 458 nm observed indicating that our hypothesis of chemical defects related to the ring-closure reaction in solid-state is a possibility. Instead as the temperature was increased two absorption maxima at 362 nm and 383 nm develop, which are consistent with the presence of fully ring-closed NDI ring-systems (see **NDI-NMe$_3$Br**, Fig. 3a). This suggests that a reversal of the base catalysed

 This journal is © The Royal Society of Chemistry 2022

Open Access Article. Published on 24 May 2022. Downloaded on 5/20/2026 3:52:14 PM.
This article is licensed under a Creative Commons Attribution 3.0 Unported Licence.

hydrolysis, shown in Fig. 2a, may occur at elevated temperatures in solution.

To determine if a ring-closing reverse hydrolysis reaction has an effect on the chemical composition of doped films, three films were drop-cast at 45 °C, 85 °C and 125 °C and then redissolved in deuterium oxide for solution NMR analysis. The ^{1}H NMR regions of the three redissolved **NDI-OH** films are compared with the solution spectra of **NDI-NMe$_3$Br** and **NDI-OH** in Fig. S9–S13 (ESI†). After drop-casting at 45 °C, a singlet at 8.29 ppm was observed, which is indicative of the reformation of four equivalent aromatic protons consistent with a ring-closed NDI. A similar singlet was observed in spectra for the 85 °C and 125 °C films (8.13 and 8.01 ppm respectively), both shifted further up-field. COSY NMR spectra of the 85 °C drop-cast film redissolved in D_2O (Fig. S14 and S15, ESI†) also shows no clear correlation between the reformed singlet and any other signal. This suggests the proton only couples to equivalent protons as is the case in symmetrical NDIs.

The integrated area of these singlets increases with temperature when compared to the peaks for the mono-hydrolysed product **6**. At drop-cast temperatures of 85 °C and higher the characteristic AB quartet and singlets, at approximately 7.70 ppm, for the two doubly hydrolysed products, **7** and **8**, were no longer observed.

The appearance, and subsequent increase in integrated peak area with drop-casting temperature, of an aromatic singlet is consistent with the reformation of the NDI ring-system through a temperature induced reversal of hydrolysis. It is therefore clear that the dynamic nature of the hydrolysis reaction led to a significant difference in the chemical composition of the films drop-cast at different temperatures. This will have to be accounted for when considering the morphology and electronic performance of the doped films. The up-field shift of the reformed aromatic peak with increasing temperature is slightly more difficult to rationalize, however. NDIs n-doped by amines have exhibited a broadening then disappearance of the NDI aromatic proton signal.[25,27] This was attributed to the formation of paramagnetic radical anions on the NDI. The shift up-field, observed in **NDI-OH** thin-films, instead indicates an increase in electron shielding through increased electron density around these aromatic protons.

Electrical conductivity of doped films

Measurement of electrical conductivity, σ, can be a useful way of judging the practical performance of doped semiconducting films. An increase in σ should also help to confirm that the changes in absorption spectra seen in Fig. 3c are due to polaron type charge carriers. In addition, conductivity measurements will provide insights into the varying chemical compositions of the films described above and how such compositional changes impact charge transport. With σ being a product of mobility, μ, and the charge carrier density, n, it can be a useful first indication of how the dynamic structure of **NDI-OH** is affecting the doping efficiency and the film morphology. Fig. 4 shows a plot of electrical conductivities as a function of drop-casting temperature used for film formation. Conductivities were measured by four-point probe in the Van der Pauw geometry at room temperature under ambient conditions.

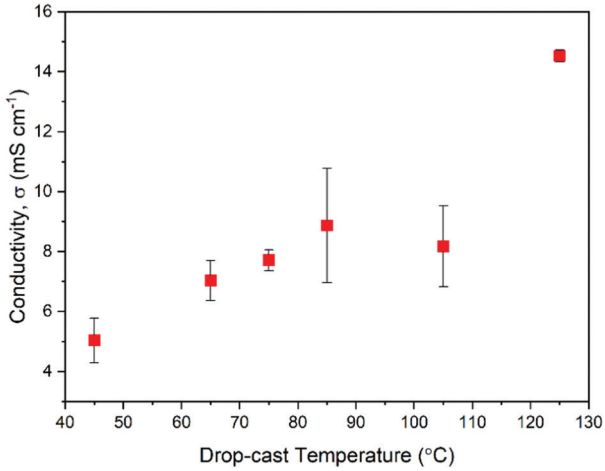

Fig. 4 Plot of thin-film conductivities of **NDI-OH** against the temperature of drop-casting used to form the film. Measurements were made at room temperature in air. Error bars were determined from film thickness measurements.

Films formed at drop-casting temperatures between 45 °C to 85 °C showed a linear increase in σ from 5.0 mS cm^{-1} to 8.9 mS cm^{-1}. The film at 105 °C however showed a slight decrease in conductivity to 8.2 mS cm^{-1} before increasing to 14.5 mS cm^{-1} when deposited at 125 °C. *I–V* curves obtained from the films (Fig. S22, ESI†) also show better ohmic behavior agreeing with the improved conductivity at higher drop-cast temperatures.

The drop in conductivity at 105 °C is initially difficult to explain. A film morphology less favorable for charge transport can lead to a decrease in mobility which in turn may be caused by the mixed chemical composition. It has also been shown that intermolecular distances can impact the generation of radical anions in NDIs bound to tertiary amines.[24] It is possible that both the hydrolysis reaction and the ammonium breakdown played a part in leading to an unfavorable morphology for charge transport and doping in films drop-cast at 105 °C. It was therefore decided that a study of the film morphology was necessary to gain a further insight into the morphological effects on electronic performance.

Morphology of doped films

Charge carrier mobility, and therefore conductivity through the doped film, is dependent on the film morphology. Furthermore, the doping mechanism and efficiency can be largely reliant on the alignment and interactions between the dopant and the semiconductor, both of which could vary greatly with film morphology.[43,44] To first image the surface morphology of the films drop-cast at different temperatures atomic force microscopy (AFM) was employed. AFM images of the six films are shown in Fig. 5. Between the drop-casting temperatures of 45 °C and 75 °C, large crystallites (approx. 2 μm in length) were observed. At 85 °C a mixed surface morphology was seen which consisted of some of the larger crystallites separated by more homogeneous and fibrous domains. At 105 °C and 125 °C the

Open Access Article. Published on 24 May 2022. Downloaded on 5/20/2026 3:52:14 PM.
This article is licensed under a Creative Commons Attribution 3.0 Unported Licence.

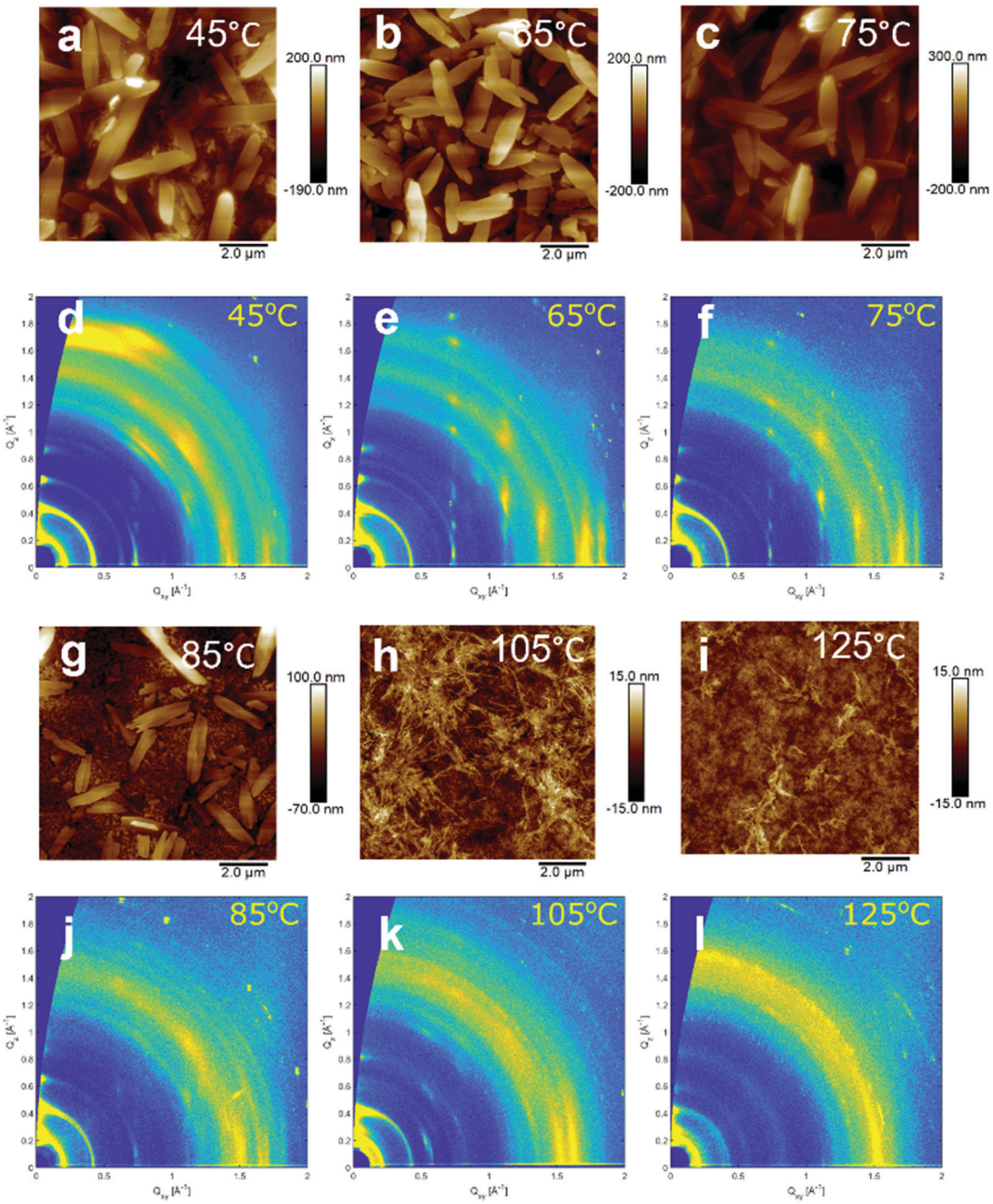

Fig. 5 AFM images (a, b, c, g, h and i) and 2D GIWAXS measurements (d, e, f, j, k and l) of **NDI-OH** films drop-cast at temperatures between 45 °C and 125 °C.

surface morphology was almost completely fibrous and seemingly continuous.

In order to determine if the bulk morphology was changing in a similar fashion, grazing incidence wide-angle X-ray scattering (GIWAXS) was performed. 2D-scattering profiles of **NDI-OH** are shown in Fig. 5. The films drop-cast at 65 °C and 75 °C showed intense and well-defined Bragg peaks. This suggests good alignment in the out-of-plane direction and indicates that the large crystallites observed in AFM images are present in the bulk. Films drop-cast at temperatures higher than 85 °C generally do not display the same crystalline order, with a loss of the Bragg peaks centred at Q_{xy} = 0.74 Å^{-1}. A new set of broad and intense Bragg peaks at Q_{xy} = 0.55 Å^{-1} were seen at drop-cast temperatures of 105 °C. This new crystalline structure is less well-textured than those seen at lower temperatures and again reflects the rise in fibrous surface morphologies seen in AFM images at temperatures above 85 °C. It is clear that both the crystalline order and the surface morphology of **NDI-OH** are drastically changed by the drop-casting temperature. This is likely due to the changing chemical composition of the film, as

 This journal is © The Royal Society of Chemistry 2022

Open Access Article. Published on 24 May 2022. Downloaded on 5/20/2026 3:52:14 PM.
This article is licensed under a Creative Commons Attribution 3.0 Unported Licence.

evidenced by NMR. Changes in morphology after doping, even in pure molecular semiconductors, are also well reported in literature.[45–47] Charge transport regimes are known to differ depending on the packing of molecules within the crystal structure, with the favourable overlap of transfer integrals (J) and higher degrees of order leading to increased mobilities.[48] The linear increase in conductivity seen between 45 °C and 75 °C can, at least partially, be explained by an increase in the crystallinity. The decrease in conductivity between 85 °C and 105 °C may be due to the disappearance of highly ordered crystalline regions between these two temperatures, although the large amount of grain boundaries between crystalline domains can be a high energetic barrier for charge carriers to cross.[49]

Electron paramagnetic resonance spectroscopy

An indication of the mobility component of the conductivity can be given by the morphological experiments above. To investigate the extent of doping, the number of polaronic unpaired electrons must be determined. Unpaired spins can be investigated through electron paramagnetic resonance (EPR) spectroscopy, where the presence of any diamagnetic species will not directly contribute to the observed signal. Generation of an anionic radical species in annealed **NDI-OH** thin-films is indicated by the single, sharp peak observed, shown in Fig. 6a. The g-factor for this film peak, and others in the series, was found to be anisotropic and closely match that of a free electron ($g_{iso} = 2.002 \pm 0.001$). No hyperfine splitting could be resolved, likely an effect of self-exchange between neutral and anionic radical **NDI-OH** species.[50,51] A significantly weaker signal was observed from an **NDI-NMe$_3$Br** thin film annealed at 45 °C compared to **NDI-OH** annealed at an analogous temperature (Fig. S18, ESI†).

The greatest signal intensity after 24 hours storage under ambient conditions occurred by drop casting **NDI-OH** at 75 °C, with general trends in signal intensity corroborating those observed by conductivity measurements. Fig. 6b shows signal intensity increase until 75 °C, where a decrease occurs and a minimum in intensity is present at 105 °C, followed by an increase at 125 °C. Such trends in radical presence also mirror morphological changes caused by annealing, shown in Fig. 5. Charge carrier mobility is less of a significant factor for EPR measurements, impacting linewidths of signals,[52] whereas charge carrier concentration will affect signal intensity. This explanation does not fully explain the minimum at 105 °C however, with competing chemical and morphological processes occurring simultaneously.

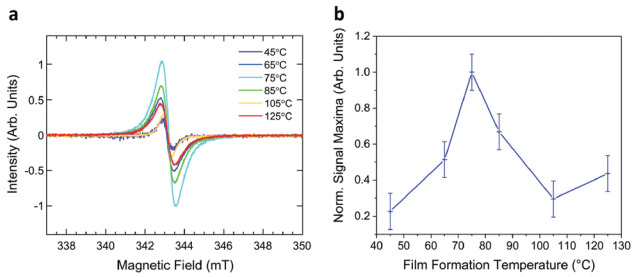

Fig. 6 (a) EPR spectrum of **NDI-OH** thin-films drop cast at temperatures between 45 °C and 125 °C. (b) General trend of radical signal intensities in **NDI-OH** thin films drop cast at temperatures between 45 °C and 125 °C, normalised to the maximum intensity observed. Measurements were taken after storage in ambient conditions for 24 h.

Identification of the doping species

The structure of the doping species and the specific chemical transformations which have occurred to generate the dopant are yet to be confirmed. With the successful doping of NDI derivatives by tertiary amines already reported,[24–27] it seems likely that the quaternary ammonium moiety degrades *via* one of two pathways. Previously it has been suggested that PDI–OH degraded by the S_N2 demethylation to generate a pendant dimethylamine moiety on the PDI core.[23] The degradation *via* an E2 Hofmann elimination to generate trimethylamine (TMA) as a dopant to rylene diimides has not been previously studied. Both computational and experimental studies have shown that the Hofmann pathway is generally favoured if β-hydrogens are available to be abstracted however.[28–31] An overview of a study in which the product of Hofmann elimination, TMA, was used to dope a neutral NDI derivative is hereby described and is briefly discussed in the ESI.†

To determine the likelihood that TMA can act as a dopant for NDI molecular semiconductors; thin films of **NDI-TEG** doped by one equivalent of TMA were made (structures in Fig. 7). Films were made by drop-casting from an aqueous solution of **NDI-TEG** and TMA (1 : 1 molar ratio). The ethylene glycol sidechains on **NDI-TEG** were used to allow solubility in water and simulate the polar environment created by charged **NDI-OH**. Initially UV-vis absorbance spectra of films formed by drop-casting at temperatures between 45 °C and 125 °C (Fig. S23 and S24, ESI†) showed only a broad absorption with maxima at approximately 350 nm.

To rule out the possibility that processing films of **NDI-OH** from a basic solution was having an effect on the identity of the dopant, solutions of **NDI-TEG** were also run through an ion-exchange column before addition of one equivalent of TMA. The absorbance spectra for these solutions are shown in Fig. 7

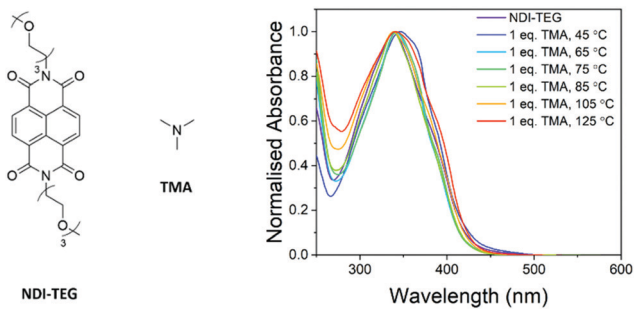

Fig. 7 Structures of **NDI-TEG** and dopant TMA (left). UV-vis absorption spectra of thin-films from blends of **NDI-TEG** and 1 equivalent trimethylamine drop-cast at temperatures between 45 °C and 125 °C (right). Solutions of **NDI-TEG** used for film formation were made basic by running through an ion-exchange column prior to addition of TMA and drop-casting.

Open Access Article. Published on 24 May 2022. Downloaded on 5/20/2026 3:52:14 PM.
This article is licensed under a Creative Commons Attribution 3.0 Unported Licence.

and show one absorption with maxima at 350 nm. Similar attempts to dope **NDI-TEG** with triethylamine were also made in order to rule out evaporation of trimethylamine from the film during drop-casting due to its low boiling point (2.9 °C). These studies are expanded upon further in the ESI.† Doping with both trimethylamine and triethylamine showed no absorption at 450 nm which was present in films of **NDI-OH** drop-cast at higher temperatures.

The lack of any evidence for doping in absorption spectra for tertiary amine doped **NDI-TEG** suggests that the active dopant in films of **NDI-OH** is not trimethylamine. In turn this adds weight to the argument that the quaternary ammonium hydroxide group decomposes *via* a demethylation[23] rather than a Hofmann elimination. With additional factors at play, such as the hydrolysis reaction, it is hard to definitively say that the active doping species is the bound dimethylamine product of demethylation. The NMR spectra of **NDI-OH** films shown in Fig. S9–S16 (ESI†) show that at higher drop-casting temperatures unidentified chemical species, beyond the products of ring-opening hydrolysis and the ring-closing reverse reaction, are present. In addition to this the ESI† shows an expansion of these NMR studies into **NDI-OH** and at least two different transformations can be seen to the NMe_3 protons of **NDI-OH** after drop-casting.

Conclusion

This study provides for the first time, detailed insights into the film formation chemistry when processing quaternary amine tethered rylene diimides. It has been shown that a reversible base catalyzed hydrolysis reaction contributes significantly to a mixed chemical composition of quaternary ammonium hydroxide self-dopants when processed as films. Through AFM and GIWAXS it could be seen that this has a pronounced effect on the film morphology. Producing films of **NDI-OH** at lower temperatures lead to a more crystalline and ordered film morphology which in turn gave a linear increase in electrical conductivity between drop-casting temperatures of 45 °C and 85 °C. Between 85 °C and 105 °C a drop in conductivity was observed which was accompanied by a change to a more fibrous and less ordered morphology. Preliminary EPR results also suggested that the spin concentration approximately followed the rise in conductivity at lower temperatures and fell between 75 °C and 105 °C.

The nature of the relationship between the film morphology, doping efficiency and the chemical composition of the films was further complicated by at least two ongoing chemical reactions at the point of film processing, the imide hydrolysis and quaternary ammonium breakdown. Gaining a more thorough understanding of these two processes, and the possibility of further chemical changes during processing, is key to identifying the active doping species in bound quaternary ammonium hydroxide n-doping systems. The water solubility and long-term ambient stability this class of materials have exhibited is rare amongst n-type organics. Although this study revealed that their mechanism of operation likely relies on a more complicated interplay of factors than assumed; beginning to control and utilize these factors will pave the way for a broader application of these promising self-dopant materials in organic electronic devices.

Author contributions

L. M. C. and B. C. S. designed the study. L. M. C., M. W., Y. D. and B. C. S. synthesized and characterised the materials. P. A. G., W. N., S. L., O. F. and C. B. N. performed the conductivity and AFM measurements. A. G., G. L. and A. S. collected and analysed the GIWAXS data. H. D. and S. H. performed the EPR experiments. All authors contributed to discussion of results and wrote the manuscript. O. F., A. S., S. H., C. B. N. and B. C. S. supervised the project.

Conflicts of interest

There are no conflicts to declare.

Acknowledgements

L. M. C. acknowledges financial support from the EPSRC (EP/N509577/1). B. C. S. acknowledges the UK Research and Innovation for Future Leaders Fellowship no. MR/S031952/1. Use of the Stanford Synchrotron Radiation Lightsource, SLAC National Accelerator Laboratory, is supported by the U.S. Department of Energy, Office of Science, Office of Basic Energy Sciences, under Contract No. DE-AC02-76SF00515. O. F. is funded by a Royal Society University Research Fellowship (UF140372 & URF/R/201013). S. H. acknowledges funding for the SPIN-lab (EP/P030548/1), and both H. D. and S. L. are funded by the EPSRC through grant EP/L016702/1.

Notes and references

1 I. E. Jacobs and A. J. Moulé, *Adv. Mater.*, 2017, **29**, 1703063.
2 Y. Lin, Y. Firdaus, M. I. Nugraha, F. Liu, S. Karuthedath, A.-H. Emwas, W. Zhang, A. Seitkhan, M. Neophytou, H. Faber, E. Yengel, I. McCulloch, L. Tsetseris, F. Laquai and T. D. Anthopoulos, *Adv. Sci.*, 2020, **7**, 1903419.
3 L. M. Cowen, J. Atoyo, M. J. Carnie, D. Baran and B. C. Schroeder, *ECS J. Solid State Sci. Technol.*, 2017, **6**, N3080–N3088.
4 W. Zhao, J. Ding, Y. Zou, C.-a Di and D. Zhu, *Chem. Soc. Rev.*, 2020, **49**, 7210–7228.
5 B. Lüssem, C.-M. Keum, D. Kasemann, B. Naab, Z. Bao and K. Leo, *Chem. Rev.*, 2016, **116**, 13714–13751.
6 D. M. de Leeuw, M. M.-J. Simenon, A. R. Brown and R. E.-F. Einerhand, *Synth. Met.*, 1997, **87**, 53–59.
7 H. Usta, C. Risko, Z. Wang, H. Huang, M. K. Deliomeroglu, A. Zhukhovitskiy, A. Facchetti and T. J. Marks, *J. Am. Chem. Soc.*, 2009, **131**, 5586–5608.

 This journal is © The Royal Society of Chemistry 2022

Open Access Article. Published on 24 May 2022. Downloaded on 5/20/2026 3:52:14 PM.
This article is licensed under a Creative Commons Attribution 3.0 Unported Licence.

8 S. Guo, S. B. Kim, S. K. Mohapatra, Y. Qi, T. Sajoto, A. Kahn, S. R. Marder and S. Barlow, *Adv. Mater.*, 2012, **24**, 699–703.
9 J. Avila, M.-G. La-Placa, E. Longhi, M. Sessolo, S. Barlow, S. R. Marder and H. J. Bolink, *J. Mater. Chem. A*, 2019, **7**, 25796–25801.
10 P. Wei, J. H. Oh, G. Dong and Z. Bao, *J. Am. Chem. Soc.*, 2010, **132**, 8852–8853.
11 M. Lu, H. T. Nicolai, G.-J. A.-H. Wetzelaer and P. W.-M. Blom, *Appl. Phys. Lett.*, 2011, **99**, 173302.
12 B. D. Naab, S. Guo, S. Olthof, E. G.-B. Evans, P. Wei, G. L. Millhauser, A. Kahn, S. Barlow, S. R. Marder and Z. Bao, *J. Am. Chem. Soc.*, 2013, **135**, 15018–15025.
13 Y. Zeng, W. Zheng, Y. Guo, G. Han and Y. Yi, *J. Mater. Chem. A*, 2020, **8**, 8323–8328.
14 C.-Y. Yang, Y.-F. Ding, D. Huang, J. Wang, Z.-F. Yao, C.-X. Huang, Y. Lu, H.-I. Un, F.-D. Zhuang, J.-H. Dou, C.-a Di, D. Zhu, J.-Y. Wang, T. Lei and J. Pei, *Nat. Commun.*, 2020, **11**, 3292.
15 B. A. Gregg and R. A. Cormier, *J. Am. Chem. Soc.*, 2001, **123**, 7959–7960.
16 B. A. Gregg, S.-G. Chen and H. M. Branz, *Appl. Phys. Lett.*, 2004, **84**, 1707–1709.
17 A. Rahmanudin, R. Marcial-Hernandez, A. Zamhuri, A. S. Walton, D. J. Tate, R. U. Khan, S. Aphichatpanichakul, A. B. Foster, S. Broll and M. L. Turner, *Adv. Sci.*, 2020, **7**, 2002010.
18 P. Luo, K. An, L. Ying, G. Li, C. Zhu, B. Fan, F. Huang and Y. Cao, *J. Mater. Chem. C*, 2020, **8**, 5273–5279.
19 F. Peng, J. Xu, Y. Zhang, R. He, W. Yang and Y. Cao, *Polym. Chem.*, 2019, **10**, 1367–1376.
20 A. M. Gaikwad, Y. Khan, A. E. Ostfeld, S. Pandya, S. Abraham and A. C. Arias, *Org. Electron.*, 2016, **30**, 18–29.
21 T. H. Reilly, A. W. Hains, H.-Y. Chen and B. A. Gregg, *Adv. Energy Mater.*, 2012, **2**, 455–460.
22 B. Russ, M. J. Robb, F. G. Brunetti, P. L. Miller, E. E. Perry, S. N. Patel, V. Ho, W. B. Chang, J. J. Urban, M. L. Chabinyc, C. J. Hawker and R. A. Segalman, *Adv. Mater.*, 2014, **26**, 3473–3477.
23 B. Russ, M. J. Robb, B. C. Popere, E. E. Perry, C.-K. Mai, S. L. Fronk, S. N. Patel, T. E. Mates, G. C. Bazan, J. J. Urban, M. L. Chabinyc, C. J. Hawker and R. A. Segalman, *Chem. Sci.*, 2016, **7**, 1914–1919.
24 Y. Matsunaga, K. Goto, K. Kubono, K. Sako and T. Shinmyozu, *Chem. – Eur. J.*, 2014, **20**, 7309–7316.
25 S. B. Schmidt, T. Biskup, X. Jiao, C. R. McNeill and M. Sommer, *J. Mater. Chem. C*, 2019, **7**, 4466–4474.
26 D. Powell, E. V. Campbell, L. Flannery, J. Ogle, S. E. Soss and L. Whittaker-Brooks, *Mater. Adv.*, 2021, **2**, 356–365.
27 S. B. Schmidt, M. Hönig, Y. Shin, M. Cassinelli, A. Perinot, M. Caironi, X. Jiao, C. R. McNeill, D. Fazzi, T. Biskup and M. Sommer, *ACS Appl. Polym. Mater.*, 2020, **2**, 1954–1963.
28 J. B. Edson, C. S. Macomber, B. S. Pivovar and J. M. Boncella, *J. Membr. Sci.*, 2012, **399-400**, 49–59.
29 S. Chempath, J. M. Boncella, L. R. Pratt, N. Henson and B. S. Pivovar, *J. Phys. Chem. C*, 2010, **114**, 11977–11983.
30 S. Chempath, B. R. Einsla, L. R. Pratt, C. S. Macomber, J. M. Boncella, J. A. Rau and B. S. Pivovar, *J. Phys. Chem. C*, 2008, **112**, 3179–3182.
31 H. Long, K. Kim and B. S. Pivovar, *J. Phys. Chem. C*, 2012, **116**, 9419–9426.
32 M. B. Kim and D. W. Dixon, *J. Phys. Org. Chem.*, 2008, **21**, 731–737.
33 Q. Sun, H. Wang, C. Yang and Y. Li, *J. Mater. Chem.*, 2003, **13**, 800–806.
34 J. Hou, Z.-a Tan, Y. Yan, Y. He, C. Yang and Y. Li, *J. Am. Chem. Soc.*, 2006, **128**, 4911–4916.
35 Y. Li in *Organic Optoelectronic Materials. Lecture Notes in Chemistry*, ed. B. Capenter, P. Ceroni, B. Kirchner, K. Landfester, J. Leszczynski, T.-Y. Luh, C. Mahlke, N. C. Polfer, R. Salzer, Springer, Cambridge, 2015, ch. 2, p. 41.
36 T. C. Barros, S. Brochsztain, V. G. Toscano, P. B. Filho and M. J. Politi, *J. Photochem. Photobiol., A*, 1997, **111**, 97–104.
37 V. Wintgens, P. Valat, J. Kossanyi, L. Biczok, A. Demeter and T. Bérces, *J. Chem. Soc., Faraday Trans.*, 1994, **90**, 411–421.
38 S. Guha and S. Saha, *J. Am. Chem. Soc.*, 2010, **132**, 17674–17677.
39 J. Li, X. Pang, Y. Wang, Y. Che and J. Zhao, *Catal. Today*, 2014, **224**, 258–262.
40 B. A. Jones, A. Facchetti, M. R. Wasielewski and T. J. Marks, *J. Am. Chem. Soc.*, 2007, **129**, 15259–15278.
41 S. Kumar, M. R. Ajayakumar, G. Hundal and P. Mukhopadhyay, *J. Am. Chem. Soc.*, 2014, **136**, 12004–12010.
42 S. Kumar and P. Mukhopadhyay, *Green Chem.*, 2018, **20**, 4620–4628.
43 K. Kang, S. Watanabe, K. Broch, A. Sepe, A. Brown, I. Nasrallah, M. Nikolka, Z. Fei, M. Heeney, D. Matsumoto, K. Marumoto, H. Tanaka, S.-i Kuroda and H. Sirringhaus, *Nat. Mater.*, 2016, **15**, 896–902.
44 J. E. Cochran, M. J.-N. Junk, A. M. Glaudell, P. L. Miller, J. S. Cowart, M. F. Toney, C. J. Hawker, B. F. Chmelka and M. L. Chabinyc, *Macromolecules*, 2014, **47**, 6836–6846.
45 J. Gao, J. D. Roehling, Y. Li, H. Guo, A. J. Moulé and J. K. Grey, *J. Mater. Chem. C*, 2013, **1**, 5638–5646.
46 R. Kroon, D. Kiefer, D. Stegerer, L. Yu, M. Sommer and C. Müller, *Adv. Mater.*, 2017, **29**, 1700930.
47 R. A. Schlitz, F. G. Brunetti, A. M. Glaudell, P. L. Miller, M. A. Brady, C. J. Takacs, C. J. Hawker and M. L. Chabinyc, *Adv. Mater.*, 2014, **26**, 2825–2830.
48 S. Fratini, M. Nikolka, A. Salleo, G. Schweicher and H. Sirringhaus, *Nat. Mater.*, 2020, **19**, 491–502.
49 L. G. Kaake, P. F. Barbara and X. Y. Zhu, *J. Phys. Chem. Lett.*, 2010, **1**, 628–635.
50 S. V. Bhosale, C. H. Jani and S. J. Langford, *Chem. Soc. Rev.*, 2008, **37**, 331–342.
51 R. L. Ward and S. I. Weissman, *J. Am. Chem. Soc.*, 1957, **79**, 2086–2090.
52 H. Matsui, Y. Takeda and S. Tokito, *Org. Electron.*, 2019, **75**, 105432.